International Journal of Thermophysics, Vol. 26, No. 1, January 2005 (© 2005)
DOI: 10.1007/s10765-005-2368-9

Opto-Thermal Mathematical Modeling and Inverse Depth Profiling Using Genetic Algorithm[1]

Y. Cui,[2] P. Xiao,[2,3] and R. E. Imhof[2]

The use of opto-thermal transient emission radiometry (OTTER) for non-invasive measurements of water concentration depth profiles in human skin is important for developing an understanding of its barrier function. In this paper, a new inverse method for analyzing opto-thermal data to yield optical depth profiles, which is based on a new multilayer mathematical model designed for opto-thermal skin data analysis, is presented. This has been combined with a novel inverse analysis technique using a genetic algorithm. The performance of the new approach is tested on both simulated data and *in vivo* experimental skin data. The theoretical background is presented, and the analysis of typical measurements using the new approach is compared with conventional analyses.

KEY WORDS: depth profiling; genetic algorithm; photothermal radiometry; skin hydration.

1. INTRODUCTION

Opto-thermal transient emission radiometry (OTTER) is a non-destructive, remote sensing measurement technology, which has proven potentially attractive for biomedical studies [1]. Our previous work has shown that the data from OTTER measurements is information rich, and one meaningful characteristic of special interest is the sample's optical depth profile, which often reflects the sample's inhomogeneity and can be correlated to concentration profiles of water or externally applied

[1]Paper presented at the Fifteenth Symposium on Thermophysical Properties, June 22–27, 2003, Boulder, Colorado, U.S.A.

[2]Faculty of ESBE, London South Bank University, 103 Borough Road, London, SE1 0AA, United Kingdom.
[3]To whom correspondence should be addressed. E-mail: xiaop@lsbu.ac.uk

0195-928X/05/0100-0213/0 © 2005 Springer Science+Business Media, Inc.

substances, depending on measurement protocol, excitation and detection wavelengths. However, due to the severe ill-posedness of the inverse calculation [2], the analysis of OTTER data is limited and scarce.

In this work, we investigate a new multilayered mathematical model and an inverse algorithm based on a genetic algorithm to extract the depth profile of the optical absorption coefficient. Good agreement of the simulated and measured data indicates reliability of the model and the algorithm.

2. MULTILAYERED MATHEMATICAL MODELING

In OTTER measurements, a pulsed laser is used as the excitation source to heat the sample, and a fast infrared detector is used as a sensor to pick up the consequent changes of the thermal radiation due to this temperature increase in the sample near surface. A schematic diagram of an OTTER measurement is shown in Fig. 1. The transient temperature field can be expressed as [3]

$$\theta(z,t)=\int_0^\infty \theta(z',0)G(z,z';t,0)dz' \tag{1}$$

where $\theta(z',0)$ is the initial temperature field and $G(z,z';t,0)$ is the Green function. The opto-thermal signal comes from the transient thermal emission, which can be calculated from

$$S(t)=\frac{\zeta B E_0}{\rho C}\int_0^\infty \beta e^{-\beta z}\theta(z,t)dz \tag{2}$$

where β is the absorption coefficient for the emitted thermal radiation, C is the specific heat, ρ is the density, E_0 is the energy density absorbed from

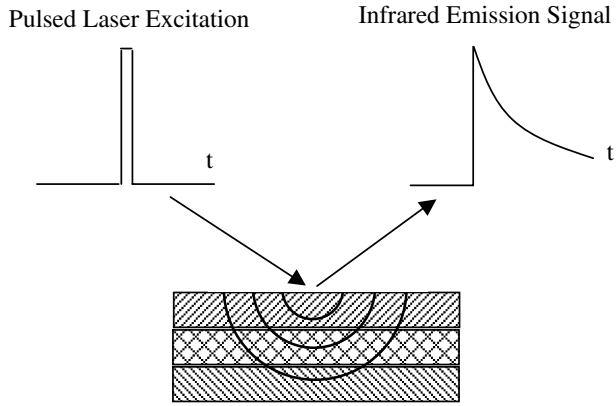

Fig. 1. Schematic diagram of OTTER measurement.

the excitation pulse, and the parameters $\zeta = \zeta(\lambda_{em})$ and B are sensitivity factors that depend on the blackbody emission curve, detector sensitivity, focusing, and alignment, but they are independent of the properties of the sample *per se* [3].

In the simplest case of a homogeneous, semi-infinite sample, the initial temperature field and the signal can be expressed, respectively, as

$$\theta(z,0) = \frac{E_0\alpha}{\rho C} e^{-\alpha z} \tag{3}$$

and

$$S(t) = \frac{\zeta B E_0 \alpha}{\rho C} e^{\alpha^2 Dt} erfc\sqrt{\alpha^2 Dt} \tag{4}$$

where α is the absorption coefficient for the excitation radiation and D is the thermal diffusivity.

But many practical samples are not sufficiently ideal enough to be treated as homogeneous, the new model discussed here is for samples with homogeneous thermal properties but with inhomogeneous optical properties. The sample is divided into N layers, which are perfectly connected with each other. Assume the absorption coefficient for excitation radiation of the sample is constant, but each layer of the sample has an absorption coefficient β_i for the emitted radiation, and a thickness of L_i. Then the signal becomes

$$\begin{aligned}
S(t) &= \frac{\zeta B E_0}{\rho C} \sum_{i=1}^{N} \int_{L_{i-1}}^{L_i} \beta_i e^{-\beta_i z} \theta(z,t) dz \\
&= \frac{E_0\alpha}{2\rho C} e^{t/\tau_\alpha} \left\{ \sum_{i=1}^{N} \frac{e^{-(\alpha+\beta_i)L_{i-1}}}{\alpha+\beta_i} erfc\left(\frac{t/\tau_\alpha - \alpha L_{i-1}/2}{\sqrt{t/\tau_\alpha}}\right) \right. \\
&\quad - \frac{e^{-(\alpha+\beta_i)L_i}}{\alpha+\beta_i} erfc\left(\frac{t/\tau_\alpha - \alpha L_i/2}{\sqrt{t/\tau_\alpha}}\right) + \frac{e^{(\beta_i^2-\alpha^2)t/\alpha^2\tau_\alpha}}{\alpha+\beta_i} \\
&\quad \times \left[erf\left(\frac{-2\beta_i t - \alpha^2 L_{i-1}\tau_\alpha}{2\alpha\sqrt{\tau_\alpha t}}\right) - erf\left(\frac{-2\beta_i t - \alpha^2 L_i \tau_\alpha}{2\alpha\sqrt{\tau_\alpha t}}\right) \right] \\
&\quad + \frac{e^{(\alpha-\beta_i)L_1}}{\alpha-\beta_i} erfc\left(\frac{t/\tau_\alpha + \alpha L_i/2}{\sqrt{t/\tau_\alpha}}\right) - \frac{e^{(\alpha-\beta_i)L_{i-1}}}{\alpha-\beta_i} erfc\left(\frac{t/\tau_\alpha + \alpha L_{i-1}/2}{\sqrt{t/\tau_\alpha}}\right) \\
&\quad \left. + \frac{e^{(\beta_i^2-\alpha^2)t/\alpha^2\tau_\alpha}}{\alpha-\beta_i} \left[erf\left(\frac{2\beta_i t + \alpha^2 L_i \tau_\alpha}{2\alpha\sqrt{\tau_\alpha t}}\right) - erf\left(\frac{2\beta_i t + \alpha^2 L_{i-1}\tau_\alpha}{2\alpha\sqrt{\tau_\alpha t}}\right) \right] \right\}
\end{aligned} \tag{5}$$

where $\tau_\alpha = 1/\left(\alpha^2 D\right)$.

In the following algorithm, all the calculations are based on the above model, normalized to its initial value $(S(t)/S(0))$.

3. INVERSE ALGORITHM

With an N-dimension vector $\vec{S}_{\mathrm{m}}$ and $\vec{S}_c\left(\vec{\beta}\right)$ $(\vec{\beta}=[\beta_1, \beta_2, \ldots, \beta_N])$ to denote the measurement signal data and calculated data, the OTTER inverse problem can be described as an optimization problem (Eq. (6)), and in terms of the property continuity of a practical biomedical sample, it is a constraint optimization problem.

$$\begin{aligned} &\text{Minimize} \left\| \vec{S}_m - \vec{S}_c\left(\vec{\beta}\right) \right\|^2 \\ &\text{subject to} \left|\beta_i - \beta_{i+1}\right| < C_\beta \quad i = 1, 2, \ldots, N \end{aligned} \tag{6}$$

where $\|\cdot\|$ denotes the Euclidean distance and C_β is a constant to maintain the property continuity of a sample.

Compared with other inverse algorithms [4], the Genetic Algorithm (GA) can be used to search complex and large-state spaces more efficiently, locate near optimal solutions more rapidly, and allow additional constraints to be easily specified [5]. Due to the flexibility and versatility of a GA in solving optimization problems, a GA is applied in this work. GAs are relatively new combinatorial search techniques based on mechanics of natural selection and natural genetics, which combines artificial survival of the fittest concept with genetic operations abstracted from nature. The basic structure of a GA is shown in Fig. 2. First, an initial population of chromosomes for the GA is generated, usually in a random way. Then, the value of a function called a fitness function is evaluated for each chromosome of the population. After this, the genetic operator's reproduction, crossover, and mutation are used in succession, to create a new population of chromosomes for the next generation. The process of evaluation and creation of new successive generations is repeated until the satisfaction of a convenient termination condition.

Conventionally, most applications of a GA to constraint optimization problems have used the penalty function approach of handling constraints [6]. However, the penalty function approach involves a number of penalty parameters that must be optimized in any problem to obtain feasible solutions. Different from the conventional methods, Deb [7] developed an efficient constraint handling method for a GA based on the penalty function approach which does not require any penalty parameter. According to his fitness function, infeasible solutions are compared based on only their constraint violation. Here, a binary GA is designed using Deb's

```
GA Procedure
begin
        gen = 0
        Initialize Pop(gen)
        Evaluate Pop(gen)
        repeat
                gen = gen+1
                Select Pop(gen) from Pop(gen-1)
                Crossover Pop(gen)
                Mutate Pop(gen)
                Evaluate Pop(gen)
                Pop(gen-1) = Pop(gen)
        until (TerminationCondition)
end
```

Fig. 2. Basic structure of a genetic algorithm.

method but with a few modifications. The fitness function is devised as follows:

$$F\left(\vec{\beta}\right)=\begin{cases}\left\|\vec{S}_m-\vec{S}_c\left(\vec{\beta}\right)\right\|^2 & \text{if } \left|\beta_i-\beta_{i+1}\right|<C_\beta\,\forall i=1,2,\ldots,N-1\\ N+\sum_{i=1}^{N-1}\left\langle C_\beta-\left|\beta_i-\beta_{i+1}\right|\right\rangle & \text{otherwise}\end{cases} \tag{7}$$

where $\langle\ \rangle$ denotes the absolute value of the operand if the operand is negative and returns a zero value otherwise. And other GA parameters are defined as follows: population size $=10N$, maximum number of generations $=100$, generation gap $=0.9$, and crossover probability $=0.7$.

4. RESULTS AND DISCUSSION

4.1. Simulation Results

With a constant thermal diffusivity and the absorption coefficient for the excitation radiation, one group of simulated data, calculated (with 5% white noise added) from one constant absorption coefficient (1.9×10^5 m^{-1}) profile for the emitted thermal radiation of a ten-layered model using Eq.(5), was used to test the new inverse algorithm. The sample is assumed to be divided equally with a 1 μm length of each layer. The results in Fig. 3 show obviously that the calculated data fit simulation signal data perfectly, and the calculated optical depth profile of β is relatively constant, which indicates that the new algorithm is efficient for the constraint handling.

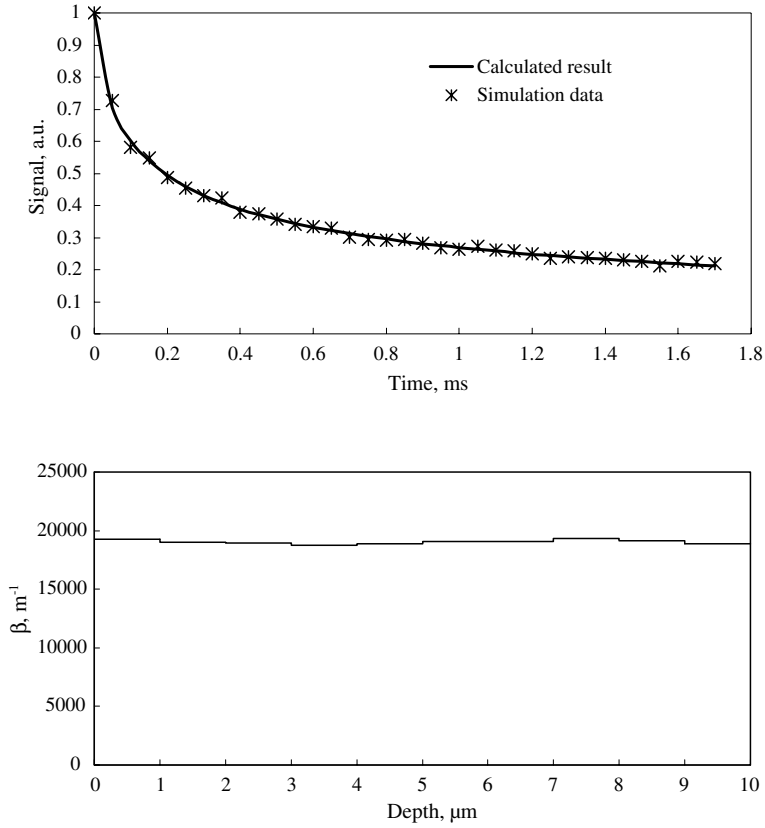

Fig. 3. Results for simulation data.

4.2. Measurement Results

The measurements were performed at different skin sites on a conventional OTTER apparatus with a Q-switched Er:YAG laser (2.94 μm) and 13.1 μm detection wavelength, and β gives information about hydration. The results are shown in Fig. 4. In general, the skin of the forearm has more water and a higher hydration gradient than other sites, while nail has the least water and lowest hydration gradient than other sites. In all sites, the skin is dry outside and wet inside, which produces a positive gradient of β. These results agree with the depth profiles obtained using the segmented least-squares fitting method [8].

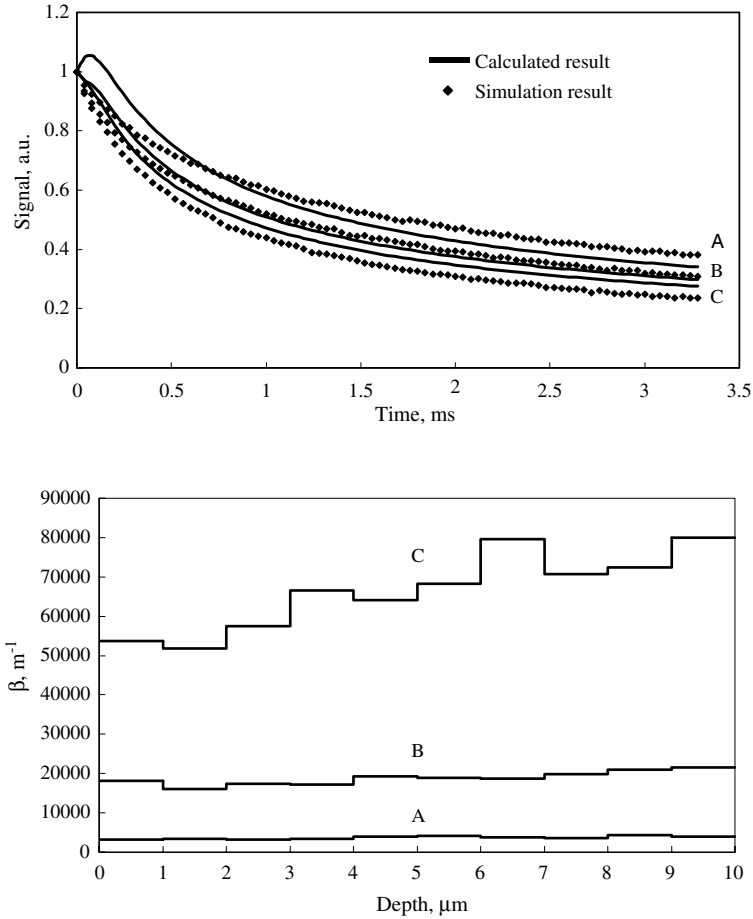

Fig. 4. Optical depth profiles of different skin sites: (A) nail, (B) palm, and (C) forearm.

5. CONCLUSIONS

We developed a new multilayer mathematical model and an opto-thermal inverse depth profiling technique using a modified GA. Both the simulation results and the measurement results agree well with the given signal data, which shows that the new scheme developed is promising and effective to solve opto-thermal inverse problems.

ACKNOWLEDGMENTS

The authors thank EPSRC, the Royal Society, and South Bank University for financial support. We also thank CVCP for the ORS award to student Y. Cui.

REFERENCES

1. R. E. Imhof, D. J. S. Birch, F. R. Thornley, J. R. Gilchrist, and T. A. Strivens, *J. Phys. E: Sci. Instrum.* **17**:512 (1984).
2. P. Xiao and R. E. Imhof, *SPIE Proc.* **3601**:340 (1999).
3. R. E. Imhof, B. Zhang, and D. J. S Birch, *Progress in Photothermal and Photoacoustic Science and Technology,* Vol. II (PTR Prentice Hall, Englewood Cliffs, New Jersey, 1994), pp. 185–236.
4. Y. Cui, P. Xiao, R. E. Imhof, and C. Glorieux, *Rev. Sci. Instrum.* **74**:368 (2003).
5. A. C. Nearchou, *Mech. Mach. Theory* **33**:273 (1998).
6. A. Homaifar, C. R. Houck, and X. Qi, *Simulation* **62**:242 (1994).
7. K. Deb, *Comput. Methods Appl. Mech. Eng.* **186**:311 (2000).
8. P. Xiao, J. A. Cowen, and R. E. Imhof, *Anal. Sci.* **17**:349 (2001).